

Cleavage of [4Fe–4S]-Type Clusters: Breaking the Symmetry

Shuqiang Niu and Toshiko Ichiye*

Department of Chemistry, Georgetown University, Washington, D.C. 20057-1227

Received: January 14, 2009; Revised Manuscript Received: March 24, 2009

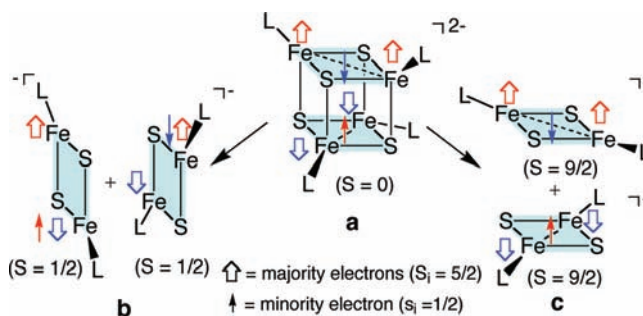
The cleavage of [4Fe–4S]-type clusters is thought to be important in proteins such as Fe–S scaffold proteins and nitrogenase. However, most [4Fe–4S]²⁺ clusters in proteins have two antiferromagnetically coupled high-spin layers in which a minority spin is delocalized in each layer, thus forming a symmetric Fe^{2.5+}–Fe^{2.5+} pair, and how cleavage occurs between the irons is puzzling because of the shared electron. Previously, we proposed a novel mechanism for the fission of a [4Fe–4S] core into two [2Fe–2S] cores in which the minority spin localizes on one iron, thus breaking the symmetry and creating a transition state with two Fe³⁺–Fe²⁺ pairs. Cleavage first through the weak Fe²⁺–S bonds lowers the activation energy. Here, we propose a test of this mechanism: break the symmetry of the cluster by changing the ligands to promote spin localization, which should enhance reactivity. The cleavage reactions for the homoligand [Fe₄S₄L₄]²⁻ (L = SCH₃, Cl, H) and heteroligand [Fe₄S₄(SCH₃)₂L₂]²⁻ (L = Cl, H) clusters in the gas phase were examined via broken-symmetry density functional theory calculations. In the heteroligand clusters, the minority spin localized on the iron coordinated by the weaker electron-donor ligand, and the reaction energy and activation barrier of the cleavage were lowered, which is in accord with our proposed mechanism and consistent with photoelectron spectroscopy and collision-induced dissociation experiments. These studies suggest that proteins requiring facile fission of their [4Fe–4S] cluster in their biological function might have spin-localized [4Fe–4S] clusters.

Introduction

The cuboidal [4Fe–4S] cluster found in metalloproteins are ubiquitous and multipurpose in biological systems.^{1–3} The most widely recognized function of iron–sulfur clusters is as electron carriers in numerous electron-transfer proteins found in bioenergetic pathways such as photosynthesis and respiration. The wide range of reduction potentials for a given cluster type appears to be mainly a function of the protein environment.^{4–12} More recently, the [4Fe–4S] core has been found to play important roles in regulation, sulfur and iron transport, and sensing.^{3,13–15} The ability of these clusters to play so many roles comes in part from variations in their unusual electronic and bonding structure. One unique feature is that the [4Fe–4S] core can be cleaved to either a [3Fe–4S] or two [2Fe–2S] cores. For instance, in the proposed mechanism for the assembly of [4Fe–4S] clusters in some proteins, a transient [4Fe–4S] cluster is assembled on cysteine residues of a scaffold protein, and then, one [2Fe–2S] layer at a time is transferred to a target protein.^{16–23} Also, the [4Fe–4S] cluster in a nitrogenase Fe–protein can convert to two [2Fe–2S] clusters.²⁴ Exploring the mechanism of the cleavage is essential in understanding the function of these proteins. Moreover, because clusters that act as redox sites are relatively stable whereas others require facile fission for their function, determining the factors that control cluster fission are crucial for understanding their structure–function relationships.

The symmetric fission of the [4Fe–4S]²⁺ core into two [2Fe–2S] cores presents an interesting conundrum because of the distinctive spin structure exhibited by the standard [Fe₄S₄(Cys)₄]²⁻ cluster found in Fe–S proteins. Mössbauer and EPR spectroscopy¹ and electronic structure calculations²⁵ support that the [4Fe–4S]²⁺ core consists of two high-spin (*S_i* = 9/2)

SCHEME 1



ferromagnetic [2Fe–2S]⁺ layers, which are coupled antiferromagnetically to form a low-spin (*S* = 0) cubic structure (Scheme 1a). In each layer, the minority spin (*s_i* = 1/2) is the highest occupied molecular orbital (HOMO) electron and is delocalized between two iron sites, which generates additional stabilizing energy and creates a symmetric Fe^{2.5+}–Fe^{2.5+} pair.²⁶ Because the antiferromagnetic coupling holding the two layers together is stronger than the spin double-exchange interactions holding a given layer together, fission by cleaving both layers in half perpendicular to the planes (Scheme 1b) should be lower in energy than fission between the layers (Scheme 1c). Moreover, cleavage between the layers would result in high-spin [2Fe–2S]⁺ cores (*S* = 9/2), contrary to experiment. However, the delocalization of the minority spin between the two irons in a layer would seem to preclude cleaving perpendicular to the layers because the spin cannot be divided evenly between the two irons, thus leading to the question of the mechanism for this cleavage reaction.

Because of the complexity of this problem, valuable insights can be provided by our broken-symmetry (BS) density functional theory (DFT) studies^{26–29} in conjunction with photoelectron spectroscopy (PES) and other experiments by Wang and

* To whom correspondence may be addressed. E-mail: ti9@georgetown.edu.

co-workers on [4Fe–4S]^{30–34} and other clusters,^{34–38} which are providing a fundamental understanding of these clusters and the effects of the protein environment on them. Because both theory and experiment are of cluster analogues in the gas phase, the DFT calculations do not require approximations for the environment such as solvent corrections or a protein matrix. In our studies of the fission of the [Fe₄S₄Cl₄]^{2–} cluster into two [Fe₂S₂Cl₂][–] clusters,^{27,28} we proposed a novel mechanism involving spin localization. In the first step, the minority spin of a layer localizes on one of the irons to create a spin-localized transition structure with Fe³⁺–Fe²⁺ pairs. Next, the two sets of weaker Fe²⁺–S bonds cleave perpendicularly to the layers to generate a half-cleaved cluster, and finally, the second set of bonds cleave to form the [2Fe–2S]⁺ products.²⁸ Thus, this mechanism implies that clusters with a lower spin double-exchange interaction, that is, greater spin-localization, should cleave more readily.

A test of this mechanism is to enhance magnitude of the minority spin localization, which should increase the reactivity to cleavage. Because a useful strategy for studying the physical origins of the effects of the protein on the properties of the clusters has been to design cluster ligands that either mimic^{39,40} or exaggerate²⁴ different types of physical interactions, ligands that break the symmetry of the layers may promote localization of the minority spin. Furthermore, [4Fe–4S] clusters in proteins that undergo facile conversion to [3Fe–4S] clusters are often coordinated by one noncysteine ligand such as an aspartate in some ferredoxins^{41–46} and water in aconitase^{3,14} pyruvate formate-lyase.⁴⁷ Interestingly, the [4Fe–4S] cluster coordinated by an *S*-adenosylmethionine (SAM)^{48–51} in the radical-SAM enzymes converts to a [3Fe–4S] cluster in pyruvate formate-lyase⁴⁷ but to one [2Fe–2S] core in biotin synthase.⁵² Moreover, a cysteine to serine mutant (C77S) of the *Chromatium vinosum* high-potential iron–sulfur protein leads to a shift in the electron cloud of the cluster toward the serine,^{53–56} indicating that ligand substitution alters the electron distribution. Thus, defining the role of ligand heterogeneity in fission not only provides a test of the mechanism but also is essential in understanding the structure–function relationships of Fe–S proteins.

Here, the mechanism was tested by breaking the symmetry of the ligation of the [4Fe–4S] cluster to promote spin localization, by utilizing BS-DFT calculations in conjunction with findings of PES and collision-induced dissociation (CID) experiments.³¹ Previous PES and DFT studies indicate that [Fe₄S₄L₄]^{2–} (L = SC₂H₅, SH, Cl, Br, I) clusters have electronic structure and other properties similar to those of the [Fe₄S₄(Cys)₄]^{2–} cluster found in proteins,²⁶ with variations due to the electron-donating ability of the terminal ligands because the minority spin is delocalized in the $\sigma_{\text{Fe–Fe}}$ orbitals, which also have $\sigma_{\text{Fe–S}}^*$ and $\sigma_{\text{Fe–L}}^*$ antibonding character.²⁶ Assuming that coordination by identical ligands on a layer promotes the delocalization of the minority spin between the irons, coordination by different ligands with different electron-donor properties may increase the localization of the minority spin on one iron by breaking the symmetry. Comparison of [Fe₄S₄(SCH₃)₂L₂]^{2–} (L = Cl, H) with [Fe₄S₄L₄]^{2–} (L = SCH₃, Cl, H) in the reactant and a half-cleaved intermediate state indicates that heteroligand coordination promotes minority spin localization and further that spin localization lowers the barrier to fission.

Methods

Because the systems here involve antiferromagnetically spin-coupled interactions, the BS approach^{57,58} for the DFT calculations⁵⁹ was employed to take these interactions into account in

the exchange–correlation energy functionals. Becke’s three-parameter hybrid exchange⁶⁰ and Lee–Yang–Parr correlation functional (B3LYP)⁶¹ with the 6-31G** basis sets^{62–64} was utilized for the geometry optimizations and electronic structure calculations of the [4Fe–4S] clusters. The calculated oxidation energies were refined at the B3LYP/6-31(++)_SG**//B3LYP/6-31G** level, where (++)_S indicates that *sp*-type diffuse functions were added to the basis set for the sulfur atoms.^{62–64} Previous studies indicate that this approach significantly improved the accuracy of the calculated redox energies.^{26,28,37} In addition, zero-point energy and entropic terms at 298 K were calculated at the B3LYP/6-31G** level. The σ -electron-donating ability of the ligands was assessed by the calculated proton affinity (PA) of the ligand alone at the B3LYP/6-31G** level; that is, ligands with greater PA should donate more σ electron density.

Transition states (TS) were optimized by an eigenvalue-following optimization method,⁶⁵ in which the final updated Hessian⁶⁶ has only one negative eigenvalue with eigenvectors representing the Fe–S bond formation and cleavage. Further optimizations along an intrinsic reaction coordinate based on the Hessian calculated above and frequency calculations were used to confirm the reaction pathways. No symmetry restraints were imposed during geometry optimizations. Although the energy of a BS state for a spin polarized low-spin state is not the energy of a pure spin state because a single determinant is used, it can be corrected by an approximate spin projection procedure.^{25,67} On the other hand, because a BS state is a weighted average of pure-spin states, the potential energy surface of a ground state with large spin numbers is close to that of the true ground state. Previous BS-DFT calculations of [Fe₂S₂(SCH₃)₄]^{2–} indicate that the projection corrected values of 2.68 Å for the Fe–Fe distance are in excellent agreement with the experimental value of 2.69 Å; however, there is no automated method for adding the projection correction to the geometry optimization, and the uncorrected value leads to a systematic increase in the Fe–Fe distance of only ~0.1 Å.⁶⁸ Moreover, the spin projection corrections tend to cancel for oxidation or reaction energies. For instance, the projection corrections on [Fe₄S₄Cl₄]^{2–} at the B3LYP/6-31(++)_SG**//B3LYP/6-31G** level lead to a decrease of 0.01 and 0.04 eV in the vertical (VDE) and adiabatic (ADE) detachment energies, respectively, which actually increases the deviation from experiment, and a decrease of 0.34 kcal/mol in the half-cleavage reaction energy. Thus, the spin projection procedures were neglected in this work.

All calculations were performed by using the NWChem program package.⁶⁹ The molecular orbital visualizations were performed by using the extensible computational chemistry environment (Ecce) application software.⁷⁰

Results and Discussion

The electronic structure of the [4Fe–4S]²⁺ core is expected to depend on the electron-donating ability of the terminal ligands because the minority spin is delocalized in the $\sigma_{\text{Fe–Fe}}$ orbitals, which also has metal–ligand antibonding character,²⁶ and the electron-donating ability should increase with decreasing PA. The calculated oxidation energies of the [4Fe–4S] clusters are in good agreement with experiment and also correlate well with the proton affinities of the ligands of [Fe₄S₄L₄]^{2–} (L = SC₂H₅[–], SH[–], Cl[–], Br[–], I[–], Figure 1). Furthermore, in a layer bonded by ligands with different PA, the Fe ligated by the poorer σ -electron donor should have less electron density and more Fe³⁺ character than the other Fe, thus breaking the symmetry

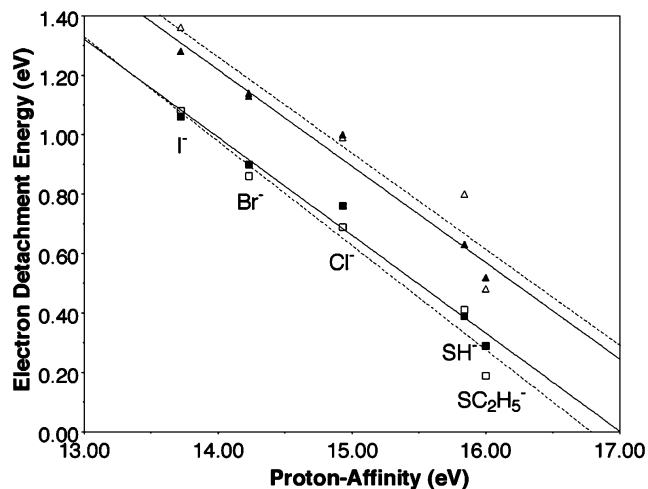
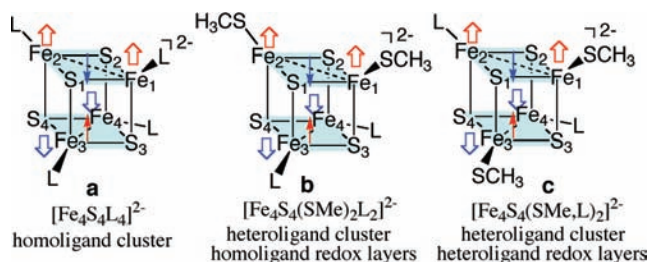


Figure 1. Calculated (dashed line) ADE (open square) and VDE (open triangle) and experimental (solid line) ADE (filled square) and VDE (filled triangle) versus PA for of $[\text{Fe}_4\text{S}_4\text{L}_4]^{2-}$ with L as indicated in the figure. In the calculations, SC_2H_5^- was replaced by a thiolate SCH_3^- group.

SCHEME 2



of the system. Consequently, the heteroligand clusters may exhibit less delocalization of the minority spin and thus greater reactivity than the homoligand clusters. A comparison is made here between the homoligand clusters $[\text{Fe}_4\text{S}_4\text{L}_4]^{2-}$ ($\text{L} = \text{SCH}_3, \text{Cl}, \text{H}$) and the heteroligand clusters $[\text{Fe}_4\text{S}_4(\text{SCH}_3)_2\text{L}_2]^{2-}$ ($\text{L} = \text{Cl}, \text{H}$, Scheme 2). Two isomers are possible for the heteroligand clusters depending on which irons the minority spins are located on, resulting in homoligand layers, denoted as $[\text{Fe}_4\text{S}_4(\text{SMe})_2\text{L}_2]^{2-}$ (Scheme 2b) or heteroligand layers, denoted as $[\text{Fe}_4\text{S}_4(\text{SMe},\text{L})_2]^{2-}$ (Scheme 2c), where SMe refers to SCH_3 . The notation $[\text{Fe}_4\text{S}_4(\text{SCH}_3)_2\text{L}_2]^{2-}$ will refer to either isomer.

Electron Detachment Energy of Cubic [4Fe–4S]. The calculated ADE and VDE of the hetero- and homoligand clusters were in good agreement with available experimental PES results (Table 1).³⁴ For $[\text{Fe}_4\text{S}_4\text{Cl}_4]^{2-}$, the weaker electron-donor chloride ligand lowered the energy of the minority spin orbitals, consequently increasing the electron detachment energy by ~ 0.5 eV with respect to $[\text{Fe}_4\text{S}_4(\text{SCH}_3)_4]^{2-}$. Conversely, for $[\text{Fe}_4\text{S}_4\text{H}_4]^{2-}$, the much better electron-donor hydride ligand decreased the detachment energy by ~ 0.6 eV with respect to $[\text{Fe}_4\text{S}_4(\text{SCH}_3)_4]^{2-}$. The calculated oxidation energies of either of the two possible isomers of the $[\text{Fe}_4\text{S}_4(\text{SCH}_3)_2\text{Cl}_2]^{2-}$ were similar to and in good agreement with experiment; however, the calculations indicate that $[\text{Fe}_4\text{S}_4(\text{SMe},\text{L})_2]^{2-}$ was slightly more stable for $\text{L} = \text{H}$ and Cl by 0.87 and 0.81 kcal/mol, respectively, than $[\text{Fe}_4\text{S}_4(\text{SMe})_2\text{L}_2]^{2-}$ (see *infra*). Overall, the detachment energy of the [4Fe–4S] cores correlated with electron-donor properties of the terminal ligands on the layer, increasing in the order $\text{HH} < \text{SMeH} < \text{SMeSMe} < \text{SMeCl} < \text{ClCl}$.

$\text{Fe}^{2.5+}$ – $\text{Fe}^{2.5+}$ versus Fe^{3+} – Fe^{2+} Character. The $\text{Fe}^{2.5+}$ – $\text{Fe}^{2.5+}$ versus Fe^{3+} – Fe^{2+} character of the layers as a function of ligand

type was examined by the length of the Fe–S bonds within a layer (Figure 2 and Supporting Information, Table S1 and S2). Previous results have shown that the BS-DFT calculations in the gas phase predict Fe–S bonds that are too long by ~ 0.05 Å, which is a systematic error when using the B3LYP functional, but show the correct trends of lengthening upon reduction from Fe^{3+} –S to Fe^{2+} –S in comparison to X-ray structures;^{26,28,37} that is, the calculated Fe^{3+} –S bond length of 2.23–2.37 Å, the $\text{Fe}^{2.5+}$ –S bond length of 2.36–2.37 Å, and the Fe^{2+} –S bond length of 2.40–2.47 Å are comparable with the experimental values of 2.20–2.27 Å,^{71,72} 2.28–2.32 Å,^{72–74} and 2.32–2.36 Å,^{71,73,75} respectively. The $\text{Fe}^{2.5+}$ – $\text{Fe}^{2.5+}$ versus Fe^{3+} – Fe^{2+} character of the layers as a function of ligand character was also examined by the Mülliken charge (Figure 3a and Supporting Information, Table S2) and the spin densities (Figure 3b and Supporting Information, Table S2) of the irons.

The clusters with a symmetric ligation pattern for each layer, that is, $[\text{Fe}_4\text{S}_4\text{L}_4]^{2-}$ and the $[\text{Fe}_4\text{S}_4(\text{SMe})_2\text{L}_2]^{2-}$ isomers, were examined first. The calculated intralayer Fe–S bonds were ~ 2.36 Å, consistent with $\text{Fe}^{2.5+}$ –S bonds. In addition, the bond lengths increased slightly with increasing electron-donating ability of the terminal ligands in the order $\text{Cl}^- < \text{SCH}_3^- < \text{H}^-$, which indicated electron-density shifting from the ligand to the iron, leading to increasing Fe^{2+} character of the Fe–S bonds (Figure 2a), in very good agreement with the experimental results (Figure 2b).^{71,73,75} Moreover, for a given Fe, the Mülliken charge decreased (Figure 3a), and the magnitude of the spin density increased (Figure 3b) with increasing Mülliken charge on its terminal ligand, indicating that electron density shifted from the ligand to the iron to increase its Fe^{2+} character. Thus, the results all indicated that the irons with terminal ligands with greater electron-donating ability had greater Fe^{2+} character, although of course the trends may be altered in a solvent environment.

The clusters with different ligands on each layer, that is, the $[\text{Fe}_4\text{S}_4(\text{SMe},\text{L})_2]^{2-}$ isomers, showed significant differences from clusters with the symmetric ligation layers. For the calculated intralayer Fe–S bonds of $[\text{Fe}_4\text{S}_4(\text{SMe},\text{Cl})_2]^{2-}$, the irons ligated by Cl^- appeared to form Fe^{2+} –S bonds, whereas the irons ligated by SCH_3^- appeared to form Fe^{3+} –S bonds, and for $[\text{Fe}_4\text{S}_4(\text{SMe},\text{H})_2]^{2-}$, the irons ligated by H^- appeared to form Fe^{3+} –S bonds, whereas the irons ligated by SCH_3^- appeared to form Fe^{2+} –S bonds (Figure 2a). This tendency is also seen in X-ray structures (Figure 2b) of other mixed ligand clusters;^{71,73,75} however, the differences in Fe–S bond length are smaller apparently because of smaller differences in electron-donating ability of the ligands in these compounds or other factors such as the aromatic phenyl group of SPh^- . Thus, heteroligand coordination on a layer apparently resulted in a set of Fe^{3+} –S and Fe^{2+} –S bonds in that layer; but unlike in the homoligand case, the Fe–S bond length decreased with increasing electron-donating ability of the ligand so that the iron coordinated with the better electron-donor ligand had greater Fe^{3+} character of its Fe–S bond than the iron coordinated with the poorer electron-donor ligand. The correlation of the Mülliken charge and the magnitude of the spin density with the $\text{Fe}^{2+}/\text{Fe}^{3+}$ character of the irons is more difficult to understand, in part because the minority spin is of opposite sign to the majority spins, so that greater spin density can mean either more electron donation from the ligand or less contribution of the minority-spin electron. However, the relative Mülliken charges and the magnitudes of the spin density of the two irons on a layer were generally consistent with the iron coordinated with the better electron-donor ligand having greater Fe^{3+} character, just as in

TABLE 1: B3LYP/6-31(++)G and Experimental Values for ADE and VDE (in eV) of the Intact [Fe₄S₄L₄]²⁻ and [Fe₄S₄(SCH₃)₂L₂]²⁻ (L = SCH₃, Cl, H; SMe = SCH₃) Clusters**

	ADE			VDE		
	L ₁ L ₂ ^a	L ₃ L ₄ ^b	exp ^c	L ₁ L ₂	L ₃ L ₄	exp ^c
[Fe ₄ S ₄ (SCH ₃) ₄] ²⁻	0.16	0.16	0.29(8) ^d	0.46	0.46	0.52(6) ^d
[Fe ₄ S ₄ Cl ₄] ²⁻	0.69	0.69	0.80(8)	0.99	0.99	1.01(6)
[Fe ₄ S ₄ H ₄] ²⁻	-0.49	-0.49		-0.12	-0.12	
[Fe ₄ S ₄ (SMe) ₂ Cl ₂] ²⁻	0.45	0.32		0.78	0.70	
[Fe ₄ S ₄ (SMe,Cl) ₂] ²⁻	0.39	0.39	0.52(8) ^d	0.74	0.74	0.71(6) ^d
[Fe ₄ S ₄ (SMe) ₂ H ₂] ²⁻	-0.16	-0.12		0.12	0.22	
[Fe ₄ S ₄ (SMe,H) ₂] ²⁻	-0.11	-0.11		0.21	0.21	

^a The electron detachment involves the layer ligated by L₁ and L₂. ^b The detachment involves the layer ligated by L₃ and L₄. ^c References 26 and 34. ^d The experimental values are for [Fe₄S₄(SC₂H₅)₄]²⁻, and the DFT calculations indicate that the detachment energies of [Fe₄S₄(SC₂H₅)₄]²⁻ are about 0.03 eV higher than those of [Fe₄S₄(SCH₃)₄]²⁻.

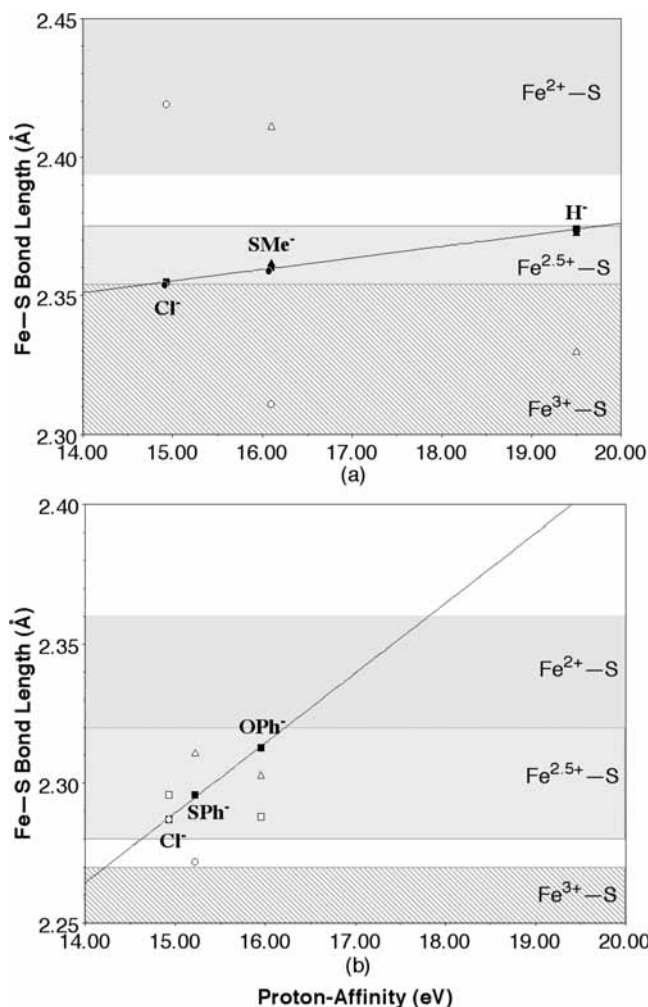


Figure 2. Scatter plot of cluster Fe–S bond lengths within the layer versus PA (a) calculated at the B3LYP/6-31G** level for [Fe₄S₄L₄]²⁻ (L = Cl, SMe₃, H; SMe = SCH₃) (filled square); [Fe₄S₄(SMe)₂L₂]²⁻, L = Cl (filled circle), H (filled triangle); and [Fe₄S₄(SMe,L)₂]²⁻, L = Cl (open circle), H (open triangle) and (b) measured by X-ray for [Fe₄S₄L₄]²⁻, L = Cl, SPh, OPh (filled square), Ph = phenyl; [Fe₄S₄(SPh,L)₂]²⁻, L = Cl (open circle), OPh (open triangle); and [Fe₄S₄(OPh,Cl)₂]²⁻ (open square). The correlation line is for the [Fe₄S₄L₄]²⁻ only.

the bond lengths. Moreover, this is consistent with the cysteine-to-serine mutation in *Chromatium vinosum* HiPIP, where the better electron-donor serine stabilizes an Fe³⁺ over an Fe^{2.5+}.^{53–56}

Moreover, along the fission pathway of the clusters, the difference in the spin densities between the two irons on a layer

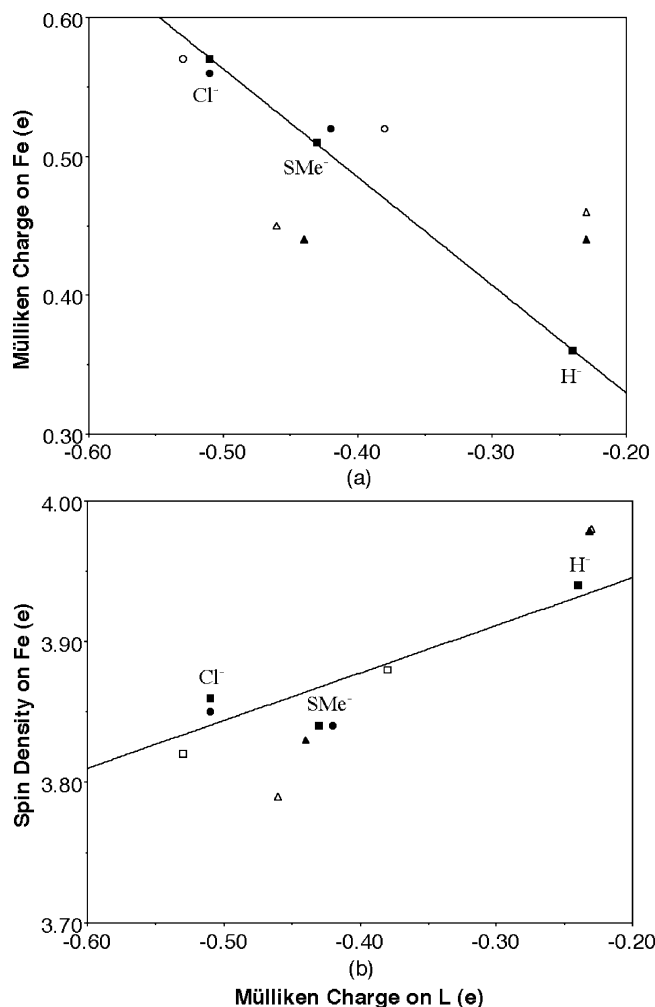


Figure 3. Scatter plot of the calculated Mulliken charge on ligand versus (a) Mulliken charge on irons and (b) Mulliken spin density on irons at the B3LYP/6-31G** level for [Fe₄S₄L₄]²⁻, L = Cl, SMe₃, H; SMe = SCH₃ (filled square); [Fe₄S₄(SMe)₂L₂]²⁻, L = Cl (filled circle), H (filled triangle); and [Fe₄S₄(SMe,L)₂]²⁻, L = Cl (open circle), H (open triangle). The correlation line is for the [Fe₄S₄L₄]²⁻ only.

of all homo- and heteroligand clusters significantly increased, consequently resulting in two Fe³⁺–Fe²⁺ pairs for the half-cleaved intermediates (Figure 4 and Supporting Information, Tables S3 and S4). Because the degree of localization for the [Fe₄S₄(SMe,L)₂]²⁻ reactant was greater and thus closer to that for its spin-localized TS (Supporting Information, Table S3), the activation barrier of the cleavage for these clusters should be lower with respect to other clusters.

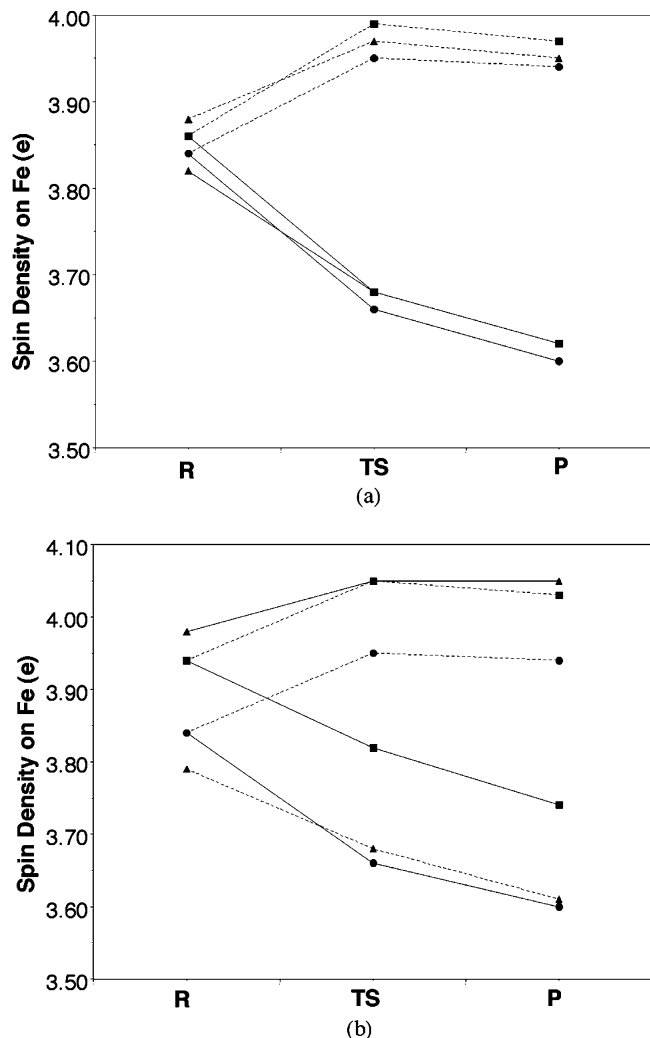
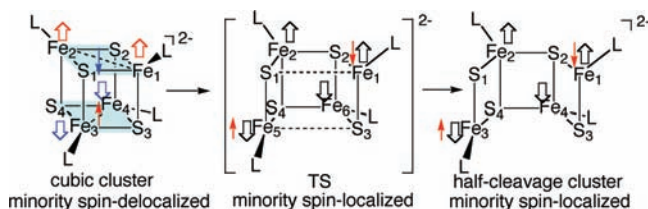


Figure 4. Change of spin density on Fe₃ (solid line) and Fe₄ (dashed line) of [Fe₄S₄L₄]²⁻, L = SMe (filled circle) and Cl (filled square), [Fe₄S₄(SMe,Cl)₂]²⁻ (filled triangle) (a) and [Fe₄S₄L₄]²⁻, L = Me (filled circle) and H (filled square), [Fe₄S₄(SMe,H)₂]²⁻ (filled triangle) (b) along cleavage reaction pathway from the cubic reactant (R) through TS to the half-cleaved product (P).

SCHEME 3



Energetics of Cleavage. The energetics of the cleavage mechanism in the heteroligand relative to homoligand clusters was examined for the steps of the cluster fission to the half-cleaved structure. Our previous DFT studies²⁸ revealed a low-barrier mechanism (Scheme 3), in which the spin-delocalized [4Fe–4S] parent goes through a spin-localized transition structure, followed by a half-cleaved cluster through cleavage perpendicular to the layers of the two weak Fe²⁺–S bonds and finally proceeds to the [2Fe–2S] fission product. However, although spin-localized intermediates for [Fe₄S₄Cl₄]²⁻ and [Fe₄S₄H₄]²⁻, in which the minority spins were excited to the spin polarized $\delta_{\text{Fe-Fe}}$ orbitals, were isolated by the BS-DFT calculations, optimization of this intermediate for [Fe₄S₄(SCH₃)₄]²⁻ fails to converge and slides smoothly to the spin-

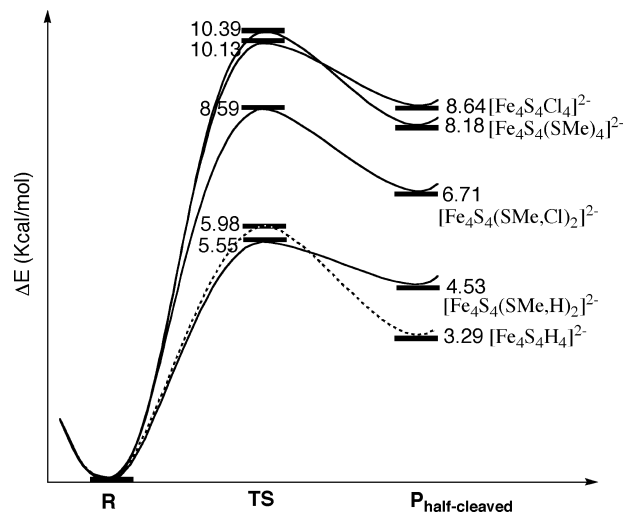


Figure 5. Calculated cleavage activation and reaction energies of [Fe₄S₄L₄]²⁻ and [Fe₄S₄(SMe,L)₂]²⁻ (L = SMe, H, Cl) along the lowest-energy pathway from the cubic reactant (R) through TS to the half-cleaved product (P).

TABLE 2: Activation Energies (ΔE^\ddagger) and Reaction Energies (ΔE) (in kcal/mol) of the Cleavage of the [Fe₄S₄L₄]²⁻ and [Fe₄S₄(SCH₃)₂L₂]²⁻ (L = SCH₃, Cl, H; SMe = SCH₃) Clusters to the Half-Cleaved Intermediate at the B3LYP/6-31G Level**

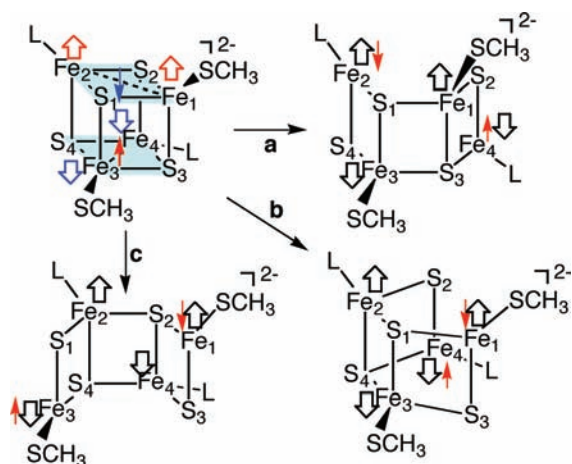
	ΔE^\ddagger	ΔG^\ddagger	ΔE	ΔG
[Fe ₄ S ₄ (SCH ₃) ₄] ²⁻	10.39	8.68	8.18	4.04
[Fe ₄ S ₄ Cl ₄] ²⁻	10.13	9.37	8.64	7.74
[Fe ₄ S ₄ H ₄] ²⁻	5.98	4.85	3.29	1.45
[Fe ₄ S ₄ (SMe) ₂ Cl ₂] ²⁻	10.46	11.44	7.94	8.00
[Fe ₄ S ₄ (SMe,Cl) ₂] ²⁻ a	8.59	8.56	6.71	4.19
[Fe ₄ S ₄ (SMe,Cl) ₂] ²⁻ b	8.62	7.95	7.49	6.39
[Fe ₄ S ₄ (SMe,Cl) ₂] ²⁻ c	11.14	10.71	10.54	9.91
[Fe ₄ S ₄ (SMe) ₂ H ₂] ²⁻	7.42	9.03	5.13	5.17
[Fe ₄ S ₄ (SMe,H) ₂] ²⁻ a	10.06	8.77	7.75	4.29
[Fe ₄ S ₄ (SMe,H) ₂] ²⁻ b	6.90	6.16	5.28	3.64
[Fe ₄ S ₄ (SMe,H) ₂] ²⁻ c	5.55	5.31	4.53	2.82

delocalized state. Further intrinsic reaction coordinate calculations and Hessian analysis of the TS optimization suggest that the cleavage of the spin-delocalized [Fe₄S₄L₄]²⁻ proceeds through a spin-localized TS directly, in which the minority spins have polarized $\sigma_{\text{Fe-Fe}}$ bonding character, to the half-cleaved structure. Thus, here, the energetics of the spin-delocalized reactant, the spin-localized TS, and the half-cleaved structure (Scheme 3) of [Fe₄S₄L₄]²⁻ and [Fe₄S₄(SCH₃)₂L₂]²⁻ (L = SCH₃, Cl, H) are compared (Table 2, Supporting Information, Table S5, and Figure 5). Both energies and free energies are reported; however, because the energies are the relevant quantities for the CID experiments, the focus is on the energies.

For the reaction to the half-cleaved species, the homoligand clusters [Fe₄S₄Cl₄]²⁻ and [Fe₄S₄(SCH₃)₄]²⁻ had similar activation energy ΔE^\ddagger of ~10 kcal/mol and reaction energy ΔE of ~8.4 kcal/mol, whereas the cleavage reaction of [Fe₄S₄H₄]²⁻ was only endothermic by 3.3 kcal/mol with a lower ΔE^\ddagger of 6.0 kcal/mol (Figure 5). The cleavage of [Fe₄S₄H₄]²⁻ was much easier than that of the other homodimers, apparently because the Fe–S bonds were longer by ~0.014–0.019 Å relative to the other homodimers.

The cleavage of heteroligand clusters was complicated by the two possible isomers, [Fe₄S₄(SMe)₂L₂]²⁻ and [Fe₄S₄(SMe,L)₂]²⁻, the latter being more stable by 0.87 and 0.81 kcal/mol for L = H and Cl, respectively. Moreover, the cleavage of

SCHEME 4



[Fe₄S₄(SMe,L)₂]²⁻ was further complicated by having three distinct cleavage pathways (Scheme 4), each with distinct reactivity and selectivity. Specifically, mechanism **a** involves cleavage through Fe₂–S₂ and Fe₄–S₄, in which the Fe are coordinated by either L = H or Cl, mechanism **c** involves cleavage through Fe₁–S₁ and Fe₃–S₃, in which the Fe are coordinated by SMe, and mechanism **b** involves cleavage through either Fe₁–S₂ and Fe₃–S₄ or Fe₂–S₁ and Fe₄–S₃, in which one Fe is coordinated by L and the other is coordinated by SMe. The pathways involving cleavage through Fe²⁺–S bonds are expected to be most favored, with spin-density patterns of the TS and half-cleaved intermediate most similar to those of the reactant.

The fission of [Fe₄S₄(SCH₃)₂Cl₂]²⁻ was first compared with that of [Fe₄S₄Cl₄]²⁻ and [Fe₄S₄(SCH₃)₄]²⁻ (Figure 5 and Table 2). The [Fe₄S₄(SMe)₂Cl₂]²⁻ isomer had one layer that looks like the [Fe₄S₄Cl₄]²⁻ layers and the other like the [Fe₄S₄(SCH₃)₄]²⁻ layers, because the ligands are symmetric for a given layer. Because the two homodimers had similar ΔE[‡], the [Fe₄S₄(SMe)₂Cl₂]²⁻ isomer also had ΔE[‡] similar to them. On the other hand, the minority spin was more localized for [Fe₄S₄(SMe,Cl)₂]²⁻ than the two homodimers, because the spin density was less on Fe₂ and Fe₄ coordinated by the Cl⁻ ligands than the other two ions, increasing their Fe²⁺ character (Figures 3 and 4). ΔE[‡] and ΔE were consistent with easier cleavage through Fe²⁺–S bonds, that is, 8.6 and 6.7 kcal/mol, respectively, for mechanism **a** with cleavage through two Fe²⁺–S bonds, slightly larger at 8.6 and 7.5 kcal/mol, respectively, for mechanism **b** with cleavage through one Fe²⁺–S bond, and with significantly larger values for mechanism **c** and the other isomer with no Fe²⁺–S bonds. Overall, the expected pathway of cleavage of [Fe₄S₄(SCH₃)₂Cl₂]²⁻ was through mechanism **a** and **b** of [Fe₄S₄(SMe,Cl)₂]²⁻ (Figure 5). Moreover, because the ΔE[‡] for these two mechanisms was about 1.5 kcal/mol lower than that of the two homodimers, cleavage of the heterodimer should be easier than that of either homodimer. In fact, fission at low collision energies (E_{CM}) is observed in CID experiments for [Fe₄S₄(SCH₃)₂Cl₂]²⁻ (at E_{CM} = 0.81 eV) but not for [Fe₄S₄(SCH₃)₄]²⁻ (E_{CM} = 0.75 eV) or for [Fe₄S₄Cl₄]²⁻.^{31,36} Fission of [Fe₄S₄Cl₄]²⁻ is observed at slightly higher energies (E_{CM} = 1.75 eV),^{31,36} but fission of [Fe₄S₄(SCH₃)₄]²⁻ is not observed until much higher energies.^{31,36}

The fission of [Fe₄S₄(SCH₃)₂H₂]²⁻ was also compared with [Fe₄S₄(SCH₃)₄]²⁻ and [Fe₄S₄H₄]²⁻. Unlike the previous case, the two homodimers differ from each other by more than 4 kcal/mol in ΔE[‡] and ΔE (Figure 5 and Table 2). However, like the

[Fe₄S₄(SMe,Cl)₂]²⁻ isomer, the [Fe₄S₄(SMe)₂H₂]²⁻ isomer had similar spin-delocalization pattern for each layer; therefore, the energetics are intermediate between the two homodimers, because one set of bonds was like one homodimer and the other set was like the other homodimer. For [Fe₄S₄(SMe,H)₂]²⁻, the spin density was significantly less on Fe₁ and Fe₃ coordinated by the H⁻ ligands than the other two irons, increasing their Fe²⁺ character (Figures 3 and 4). Here again, the ΔE[‡] and ΔE were consistent with easier cleavage through Fe²⁺–S bonds, that is, 5.6 and 4.5 kcal/mol, respectively, for mechanism **c** with cleavage through two Fe²⁺–S bonds, 6.9 and 5.3 kcal/mol for mechanism **b** with cleavage through one Fe²⁺–S bond, and much larger values for mechanism **a** and the other isomer with no Fe²⁺–S bonds. Moreover, these energies were smaller than those for chloride ligands, indicating that the greater difference in the spin density of the iron sites ligated by hydrides over those ligated by the chlorides promoted the cleavage. However, it is important to note that the effects of spin localization for either the hydride or chloride led to the greatest promotion of cleavage regardless of the nature of the ligand. Although there are no experimental results, the expected fission pathway is through mechanism **c** and **b** of [Fe₄S₄(SMe,Cl)₂]²⁻ (Figure 5 and Table 2).

Conclusions

To elucidate whether the fission of [4Fe–4S] cluster to two [2Fe–2S] clusters proceeds through a half-cleaved intermediate favored by minority spin localization, the cubic homoligand [Fe₄S₄L₄]²⁻ (L = SCH₃, Cl, H) and heteroligand [Fe₄S₄(SCH₃)₂L₂]²⁻ (L = Cl, H) clusters were investigated by using BS-DFT calculations in conjunction with results of X-ray, PES, and CID experiments. First, the results indicate that the substitution of chloride or hydride ligands for one of the two irons of a layer of [Fe₄S₄(SCH₃)₄]²⁻ causes spin localization. Thus, although the irons in a layer with two homoligands still remain a symmetric Fe^{2.5+}–Fe^{2.5+} pair, the irons in a layer with two heteroligands form a Fe³⁺–Fe²⁺ pair. Second, the Fe²⁺/Fe³⁺ character of an iron, as determined by the Fe–S bond lengths, charge density, and degree of spin localization, correlates with electron-donating ability of the ligands. In a layer with homoligands, the Fe²⁺ character of an iron slightly increases with increasing electron-donating ability of its ligand, because electron density simply shifts from the ligand to the iron. On the other hand, in a layer with heteroligands, the Fe²⁺ character of an iron significantly increases with decreasing electron-donating ability of its ligand, because even though less electron density shifts to the iron ligated by a poorer electron-donor ligand, the minority spin is attracted to it, resulting in overall greater Fe²⁺ character. Third, the reactivity of clusters in the cleavage reaction apparently correlates with the Fe²⁺ character of the Fe–S bonds. Therefore, the [Fe₄S₄(SMe,L)₂]²⁻ isomers have a lower ΔE[‡] compared to the corresponding homodimers for the lowest-energy pathway in which the two Fe–S bonds being broken have Fe²⁺ character. The results for the clusters with the chloride ligands are especially compelling, because both homoligand clusters [Fe₄S₄Cl₄]²⁻ and [Fe₄S₄(SCH₃)₄]²⁻ have approximately the same ΔE[‡], but the heteroligand cluster [Fe₄S₄(SCH₃)₂Cl₂]²⁻ is predicted to be much easier to cleave, which is consistent with the CID experimental results.³¹ Cleavage mainly via the pathway resulting in [Fe₂S₂(SCH₃)Cl]⁻ (pathway **a**) and somewhat less via the pathway resulting in [Fe₂S₂Cl₂]²⁻ and [Fe₂S₂(SCH₃)₂]⁻ (pathway **b**) is also consistent with the CID results.^{31,36}

Overall, our calculations along with the CID results support the hypothesis that the symmetric fission of [4Fe–4S] clusters

occurs via a spin localized transition structure. Furthermore, proteins requiring facile fission of their clusters for their biological function such as the scaffold proteins for Fe—S cluster assembly might have protein environments that promote spin localization. Therefore, further experimental and theoretical investigations of the effects of ligand substitution and spin localization on the cleavage of [4Fe—4S] clusters are important in elucidating the function of many [4Fe—4S] proteins.

Acknowledgment. We thank Prof. Lai-Sheng Wang, Dr. You-Jun Fu, and Dr. Xuebin Wang for the detailed experimental data and valuable discussions. This work was supported by the National Institutes of Health (GM-45303). The calculations were performed at the Environmental Molecular Sciences Laboratory, a national user facility sponsored by the U.S. DOE's Office of Biological and Environmental Research and located at Pacific Northwest National Laboratory, operated for DOE by Battelle, under the Grant GC3565 and Grant GC20901. Additional computational resources were provided by the William G. McGowan Foundation.

Supporting Information Available: Optimized geometry (Table S1) and Mülliken charges and spin density (in e^- , Table S2) of the clusters, Mülliken spin density of the TSs and half-cleaved intermediates (Tables S3 and S4), and relative isomerization energies of the heteroligand clusters (Table S5). This material is available free of charge via the Internet at <http://pubs.acs.org>.

References and Notes

- Beinert, H.; Holm, R. H.; Munck, E. *Science* **1997**, *277*, 653.
- Iron-Sulfur Proteins*; Spiro, T. G., Ed.; Wiley-Interscience: New York, 1982; Vol. IV.
- Beinert, H. *J. Biol. Inorg. Chem.* **2000**, *5*, 2.
- Adman, E.; Watenpaugh, K. D.; Jensen, L. H. *Proc. Natl. Acad. Sci. U.S.A.* **1975**, *72*, 4854.
- Kassner, R. J.; Yang, W. *J. Am. Chem. Soc.* **1977**, *99*, 4351.
- Stephens, P. J.; Jollie, D. R.; Warshel, A. *Chem. Rev.* **1996**, *96*, 2491.
- Sheridan, R. P.; Allen, L. C.; Carter, C. W. *J. Biol. Chem.* **1981**, *256*, 5052.
- Backes, G.; Mino, Y.; Loehr, T. M.; Meyer, T. E.; Cusanovich, M. A.; Sweeny, W. V.; Adman, E. T.; Sanders-Loehr, J. *J. Am. Chem. Soc.* **1991**, *113*, 2055.
- Banci, L.; Bertini, I.; Gori Savellini, G.; Luchinat, C. *Inorg. Chem.* **1996**, *35*, 4248.
- Babini, E.; Borsari, M.; Capozzi, F.; Eltis, L. D.; Luchinat, C. *J. Biol. Inorg. Chem.* **1999**, *4*, 692.
- Beck, B. W.; Xie, Q.; Ichiye, T. *Biophys. J.* **2001**, *81*, 601.
- Glaser, T.; Bertini, I.; Moura, J. J.; Hedman, B.; Hodgson, K. O.; Solomon, E. I. *J. Am. Chem. Soc.* **2001**, *123*, 4859.
- Beinert, H.; Kiley, P. J. *Curr. Opin. Chem. Biol.* **1999**, *3*, 152.
- Beinert, H.; Kennedy, M. C.; Stout, C. D. *Chem. Rev.* **1996**, *96*, 2335.
- Flint, D. H.; Allen, R. M. *Chem. Rev.* **1996**, *96*, 2315.
- Krebs, C.; Agar, J. N.; Smith, A. D.; Frazzon, J.; Dean, D. R.; Huynh, B. H.; Johnson, M. K. *Biochem.* **2001**, *40*, 14069.
- Smith, A. D.; Jameson, G. N.; Dos Santos, P. C.; Agar, J. N.; Naik, S.; Krebs, C.; Frazzon, J.; Dean, D. R.; Huynh, B. H.; Johnson, M. K. *Biochem.* **2005**, *44*, 12955.
- Agar, J. N.; Krebs, C.; Frazzon, J.; Huynh, B. H.; Dean, D. R.; Johnson, M. K. *Biochem.* **2000**, *39*, 7856.
- Ding, H.; Clark, R. J. *Biochem. J.* **2004**, *379*, 433.
- Ding, H.; Clark, R. J.; Ding, B. *J. Biol. Chem.* **2004**, *279*, 37499.
- Wollenberg, M.; Berndt, C.; Bill, E.; Schwenn, J. D.; Seidler, A. *Eur. J. Biochem.* **2003**, *270*, 1662.
- Berndt, C.; Lillig, C. H.; Wollenberg, M.; Bill, E.; Mansilla, M. C.; de Mendoza, D.; Seidler, A.; Schwenn, J. D. *J. Biol. Chem.* **2004**, *279*, 7850.
- Dos Santos, P. C.; Smith, A. D.; Frazzon, J.; Cash, V. L.; Johnson, M. K.; Dean, D. R. *J. Biol. Chem.* **2004**, *279*, 19705.
- Sen, S.; Igarashi, R.; Smith, A.; Johnson, M. K.; Seefeldt, L. C.; Peters, J. W. *Biochem.* **2004**, *43*, 1787.
- Noodleman, L.; Peng, C. Y.; Case, D. A.; Mousesca, J. M. *Coord. Chem. Rev.* **1995**, *144*, 199.
- Wang, X.-B.; Niu, S.-Q.; Yang, X.; Ibrahim, S. K.; Pickett, C. J.; Ichiye, T.; Wang, L.-S. *J. Am. Chem. Soc.* **2003**, *125*, 14072.
- Yang, X.; Wang, X.-B.; Niu, S.; Pickett, C. J.; Ichiye, T.; Wang, L.-S. *Phys. Rev. Lett.* **2002**, *89*, 163401.
- Niu, S.-Q.; Wang, X.-B.; Yang, X.; Wang, L.-S.; Ichiye, T. *J. Phys. Chem. A* **2004**, *108*, 6750.
- Niu, S.-Q.; Ichiye, T. *Theor. Chim. Acta* **2007**, *117*, 275.
- Yang, X.; Wang, X. B.; Wang, L. S. *Int. J. Mass. Spectrom.* **2003**, *228*, 797.
- Fu, Y. J.; Laskin, J.; Wang, L. S. *Int. J. Mass. Spectrom.* **2006**, *255*, 102.
- Fu, Y. J.; Laskin, J.; Wang, L. S. *Int. J. Mass. Spectrom.* **2007**, *263*, 260.
- Zhai, H. J.; Yang, X.; Fu, Y. J.; Wang, X. B.; Wang, L. S. *J. Am. Chem. Soc.* **2004**, *126*, 8413.
- Fu, Y. J.; Yang, X.; Wang, X. B.; Wang, L. S. *Inorg. Chem.* **2004**, *43*, 3647.
- Fu, Y. J.; Niu, S.-Q.; Ichiye, T.; Wang, L.-S. *Inorg. Chem.* **2005**, *44*, 1202.
- Fu, Y. J.; Yang, X.; Wang, X. B.; Wang, L. S. *J. Phys. Chem. A* **2005**, *109*, 1815.
- Niu, S.-Q.; Wang, X.-B.; Nichols, J. A.; Wang, L.-S.; Ichiye, T. *J. Phys. Chem. A* **2003**, *107*, 2898.
- Niu, S.-Q.; Nichols, J. A.; Ichiye, T. *J. Chem. Theory Comput.* **2009**, in press.
- Yang, X.; Niu, S. Q.; Ichiye, T.; Wang, L. S. *J. Am. Chem. Soc.* **2004**, *126*, 15790.
- Fu, Y. J.; Niu, S. Q.; Yang, X.; Wang, X. B.; Ichiye, T.; Wang, L. S., unpublished.
- George, S. J.; Armstrong, F. A.; Hatchikian, E. C.; Thomson, A. J. *Biochem. J.* **1989**, *264*, 275.
- Thomson, A. J.; Breton, J.; Butt, J. N.; Hatchikian, E. C.; Armstrong, F. A. *J. Inorg. Biochem.* **1992**, *47*, 197.
- Conover, R. C.; Kowal, A. T.; Fu, W. G.; Park, J. B.; Aono, S.; Adams, M. W.; Johnson, M. K. *J. Biol. Chem.* **1990**, *265*, 8533.
- Gorst, C. M.; Yeh, Y. H.; Teng, Q.; Calzolari, L.; Zhou, Z. H.; Adams, M. W.; La Mar, G. N. *Biochem.* **1995**, *34*, 600.
- Calzolari, L.; Gorst, C. M.; Zhao, Z. H.; Teng, Q.; Adams, M. W.; La Mar, G. N. *Biochem.* **1995**, *34*, 11373.
- Busch, J. L.; Breton, J. L.; Bartlett, B. M.; Armstrong, F. A.; James, R.; Thomson, A. J. *Biochem. J.* **1997**, *323*, 95.
- Walsby, C. J.; Ortillo, D.; Yang, J.; Nnyepi, M. R.; Broderick, W. E.; Hoffman, B. M.; Broderick, J. B. *Inorg. Chem.* **2005**, *44*, 727.
- Cheek, J.; Broderick, J. B. *J. Biol. Inorg. Chem.* **2001**, *6*, 209.
- Fontecave, M.; Mulliez, E.; Ollagnier-de-Choudens, S. *Curr. Opin. Chem. Biol.* **2001**, *5*, 506.
- Jarrett, J. T. *Curr. Opin. Chem. Biol.* **2003**, *7*, 174.
- Frey, P. A.; Magnusson, O. T. *Chem. Rev.* **2003**, *103*, 2129.
- Jarrett, J. T. *Arch. Biochem. Biophys.* **2005**, *433*, 312.
- Dilg, A. W. E.; Capozzi, F.; Mentler, M.; Iakovleva, O.; Luchinat, C.; Bertini, I.; Parak, F. G. *J. Biol. Inorg. Chem.* **2001**, *6*, 232.
- Dilg, A. W. E.; Grantner, K.; Iakovleva, O.; Parak, F. G.; Babini, E.; Bertini, I.; Capozzi, F.; Luchinat, C.; Meyer-Klaucke, W. *J. Biol. Inorg. Chem.* **2002**, *7*, 691.
- Dilg, A. W. E.; Mincione, G.; Achterhold, K.; Iakovleva, O.; Mentler, M.; Luchinat, C.; Bertini, I.; Parak, F. G. *J. Biol. Inorg. Chem.* **1999**, *4*, 727.
- Babini, E.; Bertini, I.; Borsari, M.; Capozzi, F.; Dikiy, A.; Eltis, L. D.; Luchinat, C. *J. Am. Chem. Soc.* **1996**, *118*, 75.
- Noodleman, L. *J. Chem. Phys.* **1981**, *74*, 5737.
- Noodleman, L.; Case, D. A. *Adv. Inorg. Chem.* **1992**, *38*, 423.
- Parr, R. G.; Yang, W. *Density-functional theory of atoms and molecules*; Oxford University Press: Oxford, U.K., 1989.
- Becke, A. D. *J. Chem. Phys.* **1993**, *98*, 5648.
- Lee, C. T.; Yang, W. T.; Parr, R. G. *Phys. Rev. B* **1988**, *37*, 785.
- Rassolov, V. A.; Pople, J. A.; Ratner, M. A.; Windus, T. L. *J. Chem. Phys.* **1998**, *109*, 1223.
- Francil, M. M.; Petro, W. J.; Hehre, W. J.; Binkley, J. S.; Gordon, M. S.; DeFrees, D. J.; Pople, J. A. *J. Chem. Phys.* **1982**, *77*, 3654.
- Hariharan, P. C.; Pople, J. A. *Theor. Chim. Acta* **1973**, *28*, 213.
- Schlegel, H. B. *J. Comput. Chem.* **1982**, *3*, 214.
- Foresman, J. B.; Frisch, A. *Exploring chemistry with electronic structure methods*, 2nd ed.; Gaussian Inc.: Pittsburgh, 1996.
- Mousesca, J. M.; Chen, J. L.; Noodleman, L.; Bashford, D.; Case, D. A. *J. Am. Chem. Soc.* **1994**, *116*, 11898.
- Li, J. *Acta Chimica Sinica* **2000**, *58*, 1529.
- Straatsma, T. P.; Aprà, E.; Windus, T. L.; Bylaska, E. J.; de Jong, W.; Hirata, S.; Valiev, M.; Hackler, M.; Pollack, L.; Harrison, R.; Dupuis, M.; Smith, D. M. A.; Nieplocha, J. V. T.; Krishnan, M.; Auer, A. A.; Brown, E.; Cisneros, G.; Fann, G.; Früchtl, H.; Garza, J.; Hirao, K.; Kendall, R.; Nichols, J.; Tsemekhman, K.; Wolinski, K.; Anchell, J.; Bernholdt, D.;

Borowski, P.; Clark, T.; Clerc, D.; Dachselt, H.; Deegan, M.; Dyllal, K.; Elwood, D.; Glendening, E.; Gutowski, M.; Hess, A.; Jaffe, J.; Johnson, B.; Ju, J.; Kobayashi, R.; Kutteh, R.; Lin, Z.; Littlefield, R.; Long, X.; Meng, B.; Nakajima, T.; Niu, S.; Rosing, M.; Sandrone, G.; Stave, M.; Taylor, H.; Thomas, G.; van Lenthe, J.; Wong, A.; Zhang, Z. *NWChem, A Computational Chemistry Package for Parallel Computers, Version 4.6*; Pacific Northwest National Laboratory: Richland, Washington, 2004.

(70) Black, G.; Didier, B.; Elsethagen, T.; Feller, D.; Gracio, D.; Hackler, M.; Havre, S.; Jones, D.; Jurrus, E.; Keller, T.; Lansing, C.; Matsumoto, S.; Palmer, B.; Peterson, M.; Schuchardt, K.; Stephan, E.; Taylor, H. T., G.; Vorpapel, E.; Windus, T.; Winters, C. *Ecce, A Problem Solving*

Environment for Computational Chemistry, Software Version 3.2.1; Pacific Northwest National Laboratory: Richland, Washington, 2004.

(71) Lane, R. W.; Ibers, J. A.; Frankel, R. B.; Papaefthymiou, G. C.; Holm, R. H. *J. Am. Chem. Soc.* **1977**, *99*, 84.

(72) Carney, M. J.; Papaefthymiou, G. C.; Spertalian, K.; Frankel, R. B.; Holm, R. H. *J. Am. Chem. Soc.* **1988**, *110*, 6084.

(73) Osullivan, T.; Millar, M. M. *J. Am. Chem. Soc.* **1985**, *107*, 4096.

(74) Excoffon, P.; Laugier, J.; Lamotte, B. *Inorg. Chem.* **1991**, *30*, 3075.

(75) Venkateswara Rao, P.; Holm, R. H. *Chem. Rev.* **2004**, *104*, 527.

JP900402Y